Design and Analysis of a Compliant Parallel Pan-Tilt Platform

Jingjun Yu [1]*, Dengfeng Lu[1], Guangbo Hao[2]

[1] Robotics Institute, Beihang University, Beijing, 100191, China

[2] School of Engineering, University College Cork, Cork, Ireland

*E-mail: jjyu@buaa.edu.cn

Abstract: In combination of the advantages of both parallel mechanisms and compliant mechanisms, a compliant parallel mechanism with two rotational DOFs (degrees of freedom) is designed to meet the requirement of a lightweight and compact pan-tilt platform. Firstly, two commonly-used design methods i.e. direct substitution and FACT (Freedom and Constraint Topology) are applied to design the configuration of the pan-tilt system, and similarities and differences of the two design alternatives are compared. Then inverse kinematic analysis of the candidate mechanism is implemented by using the pseudo-rigid-body model (PRBM), and the Jacobian related to its differential kinematics is further derived to help designer realize dynamic analysis of the 8R compliant mechanism. In addition, the mechanism's maximum stress existing within its workspace is tested by finite element analysis. Finally, a method to determine joint damping of the flexure hinge is presented, which aims at exploring the effect of joint damping on actuator selection and real-time control. To the authors' knowledge, almost no existing literature concerns with this issue.

Keywords: Compliant parallel mechanism, Pan-tilt, Flexure hinge, Joint damping

1 Introduction

With the rapid development of computer and control technology, UAVs (unmanned aerial vehicles) that install visual tracking equipments come into being. They are capable of monitoring the ground or low altitude and are therefore widely used in various fields, such as aerial photography, geodetic survey, highway cruising, and disaster relief. In general, cameras of UAVs are installed upon a pan-tilt device with two or three rotational DOFs (degrees of freedom), which enhance its capability to track the target. As one of important parts of an UAV, the performances of the pan-tilt platform will directly affect the UAV's quality to execute tasks. In recent years, it is particularly necessary to design a simple, universal, lightweight and compact pan-tilt system.

Currently, most of pan-tilt systems are essentially a rigid serial universal joint mechanism. They are simple, but have some disadvantages including complex installation, slow-response, large drive torque of joints closer to the base. Considering the fact that compliant mechanisms are free assembly, free lubrication, no backlash [1-2], and parallel mechanisms have fast

response, high stiffness, high bearing capacity, and simple inverse kinematics [3-4], it is instead tried to design a compliant parallel mechanism as the pan-tilt device. The fundamental requirements for this kind of new pan-tilt device include a pitch angle range of ±10°, a phase angle range of 0~360°, and a simple lightweight structure as well.

In this paper, a design paradigm of 2-DOF compliant parallel pan-tilt platform is presented. The whole paper is organized as follows: Section 2 elaborates the design approach and process of the compliant parallel system. In Section 3, kinematics of the compliant parallel mechanism is analyzed based on the pseudo-rigid-body model (PRBM). Furthermore, the maximum stress of the mechanism is tested. In Section 4, the method to determine joint damping of the flexure hinge is introduced and how joint damping affects actuator selection and real-time control is finally explored.

2 Conceptual Design of 2-DOF Compliant Parallel Rotational Mechanisms

Many researches [5-10] have concerned about the design of compliant parallel mechanisms. In general, two methods are commonly used to design this kind of mechanism. One is the direct substitution for the existing rigid parallel counterparts. For example, Hara [5] designed a 6-DOF compliant micro-positioning platform, whose configuration is a 6-SPS (S: spherical joint; P: prismatic joint) structure with the same type as the Stewart platform. The other is the Freedom and Constraint Topology (FACT) approach [11-12] evolved from screw theory [13]. For example, a compliant parallel guiding stage can be composed of two parallel sheets and two rigid bodies. In the following, these two methods are used to design pan-tilt devices and the resultant configurations obtained from different methods are compared.

2.1 Direct Substitution Method

Direct substitution Method is established upon the existing rigid parallel mechanism, in which all kinematic pairs are replaced by flexure hinges [14] or compliant joints [15]. As a result, some practical compliant parallel mechanisms might be found after attempts. By referring to some literatures, dozens of parallel mechanisms with two rotational DOFs are acquired, such as spherical 5R (R: revolute) parallel mechanism [16-17], 8R (RRR-RR-RRR) mechanism [18-19], Omni Wrist III [20] and its derivatives [21]. Due to its characteristics of simple structure and outstanding performances, the RRR-RR-RRR mechanism (hereinafter referred to 8R mechanism) is chosen as the final mechanism that would be substituted. In the 8R mechanism illustrated in Fig. 1, all three limbs are identical, the angle between the button joint and the middle joint is 90° and the angle θ_0 between the top joint and the middle joint is 60° within each limb. The orientation of the moving platform is determined by the pitch angle γ and the phase angle α.

Next, notch flexure hinges are used to replace all kinematic joints in the 8R mechanism (Fig. 1). In general, there are four types of notch flexure hinges which are commonly used.

They are circular notch flexure hinge, elliptic notch flexure hinge, prismatic beam flexure hinge, and corner-filleted flexure hinge, which are detailed in literatures [22-23]. By comparing these four types of notch flexure hinges, it is concluded that corner-filleted flexure hinge has a relatively low precision, but a large travel, which makes it suitable as the joint of the compliant pan-tilt device. The 8R mechanism whose joints are replaced by corner-filleted flexure hinges (Fig. 2) is called 8R compliant mechanism, as shown in Fig. 3. Eight flexure hinges in 8R compliant mechanism is denoted by joint J_i (i =1, 2, …, 8), and the axial length of joint J_i is a_i (i=1, 2, …, 8).

DOF characteristic of the resultant compliant mechanism is tested by means of the modal analysis. Given the size of the pan-tilt platform, i.e. the parameters of the 8R compliant mechanism are chosen as follows: a_1=a_2=a_3=40 mm, a_4=a_5=65 mm, a_6=55 mm, a_7=70 mm, a_8=48 mm. In view of travel range and precision of the pan-tilt device, parameters of flexure hinge are chosen as follows: h=15 mm, t=10 mm, l=5 mm, R=1.75 mm, δ=0.6 mm. Modal analysis with aid of finite element software ANSYS is used to analyze natural frequencies of the 8R compliant mechanism, whose the first six natural frequencies are listed in Table 1. It is shown from Table 1 that the first and the second natural frequencies are closer and far less than the third natural frequency, which verifies that the 8R compliant mechanism has two DOFs. The first two mode shapes of the 8R compliant mechanism, as shown in Fig. 4, reflect its two rotational DOFs, respectively.

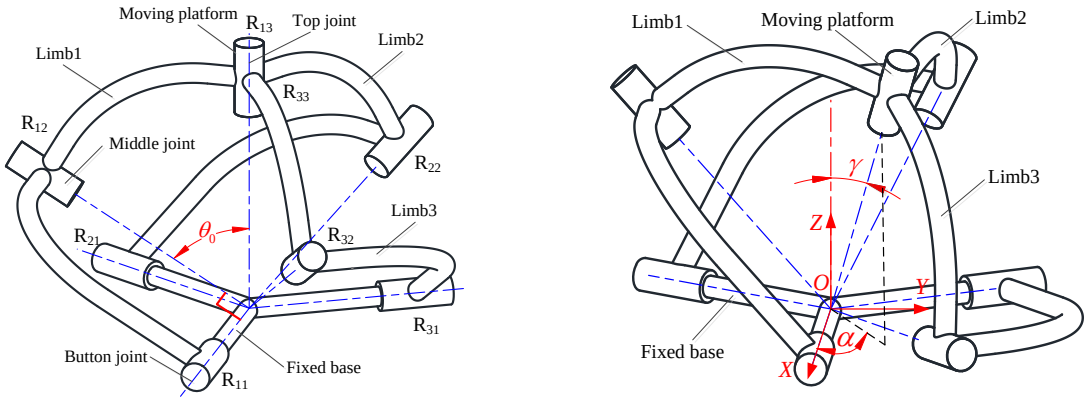

(a) Initial configuration (R_{13} and R_{33} share the same axis) (b) General configuration

Fig. 1 Configuration of the 8R spherical rigid mechanism

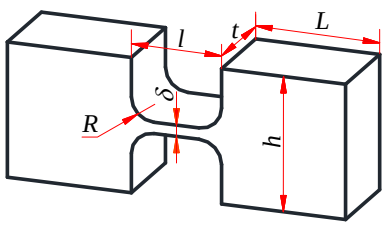

Fig. 2 Geometric parameters of corner-filleted flexure hinge

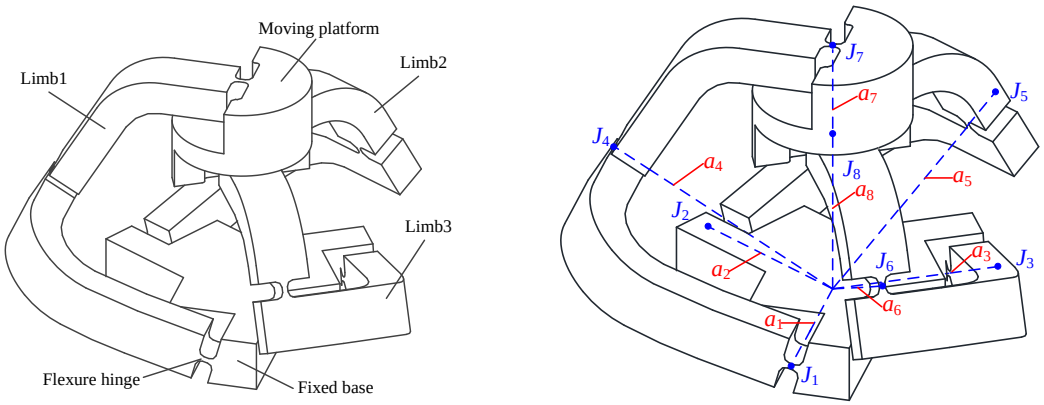

(a) Configuration (b) Geometrical parameters

Fig. 3 The 8R compliant mechanism obtained by using the substitution method

Table 1 The first six natural frequencies of the 8R compliant mechanism

Order of natural frequency	1	2	3	4	5	6
Value of natural frequency/Hz	24.4	27.4	79.9	132.7	146.0	200.2

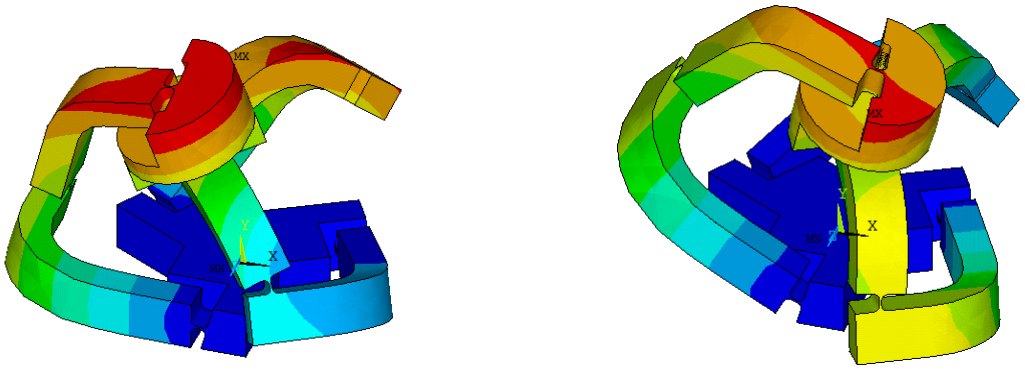

(a) The first order mode (b) The second order mode

Fig. 4 Mode shapes of the 8R compliant parallel mechanism corresponding to the first and the second natural frequencies respectively

2.2 FACT Approach

In the design of compliant parallel mechanism, the FACT approach can be selected as an important guiding tool because it helps designers figure out the desired configuration in a rapid and visual way. There are totally three steps in the FACT design process. Firstly, freedom space of the specified mechanism is depicted as a line pattern. Secondly, according to the FACT approach, constraint space of the mechanism is determined uniquely and also depicted as another line pattern. Finally, the expected configuration could be obtained based on the constraint space. The whole design process of the compliant parallel mechanism with two rotational DOFs is illustrated in Fig. 5.

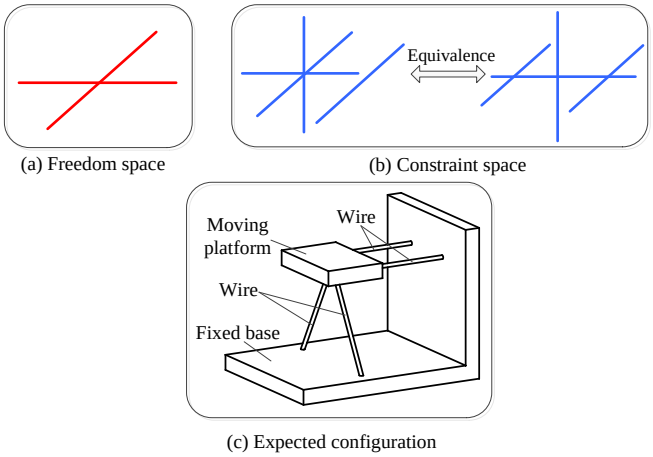

Fig. 5 Obtain a 2-DOF Compliant mechanism by using FACT approach

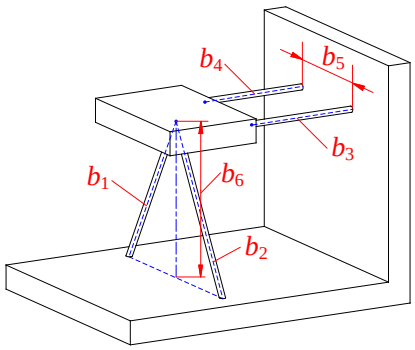

Fig. 6 Geometrical parameters of the compliant mechanism composed by wire flexures

Geometrical parameters of the resultant compliant parallel mechanism are illustrated in Fig. 6. The length of the wire flexures in the mechanism are denoted as b_j (j=1, 2… 6). The overall size of the mechanism should be similar to that of the 8R compliant mechanism mentioned previously. So, b_1=b_2=70 mm, b_3=b_4=50 mm, b_5=40 mm, b_6=60 mm, and the diameter of circular cross section of the wire flexures is 2.5mm.

Modal analysis with aid of ANSYS is also used to acquire the first six natural frequencies of the second compliant parallel mechanism and the results are listed in Table 2. The mode shapes corresponding to the first and the second natural frequencies are shown in Fig. 7. By analyzing the results, it verifies that the mechanism in Fig. 5 also has two rotational DOFs. However, the first and the second natural frequencies listed in Table 2 are not much smaller than the third one. Consequently, the parameters of the second compliant parallel mechanism need to be optimized.

Table 2 Natural frequencies of the compliant mechanism composed by wire flexures

Order of natural frequency	1	2	3	4	5	6
Value of natural frequency /Hz	76.2	160.7	307.8	529.1	688.7	706.5

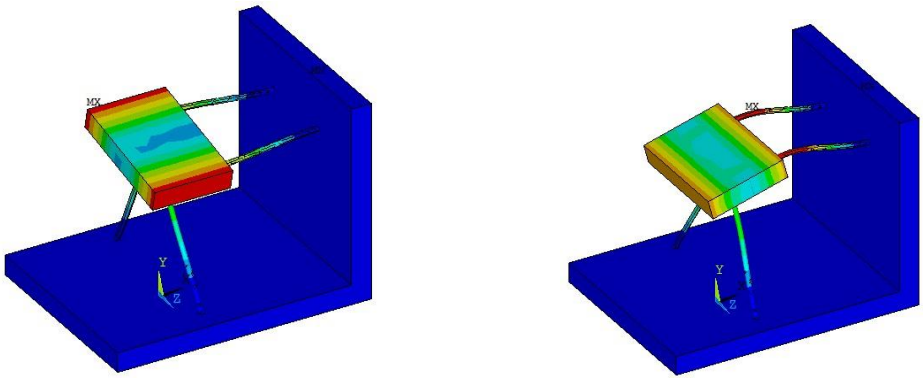

(a) The first order mode (b) The second order mode

Fig. 7 Mode shapes corresponding to the first and the second natural frequencies of the compliant mechanism using FACT approach

Although both two mechanisms shown in Fig. 3 and Fig. 5 have identical DOF characteristic, their configurations vary clearly because of their different guiding topology. For the mechanism in Fig. 3, kinematic pairs in each limb are arranged in series and the resultant DOF of the moving platform increases. However, for the mechanism in Fig. 5, with the number of limbs increases, DOF of the moving platform decreases due to introduction of more constraints. There exists a large difference between the two kinds of mechanisms from the point of actuator arrangement as well. For the mechanism in Fig. 3, the moving platform would reach any position within the workspace when two actuators are imposed upon any two button joints respectively, for the mechanism in Fig. 5, however, it needs the extra decoupling mechanisms to work with the actuators. As a result, the mechanism in Fig. 3 seems more complex, but it is suitable as an active mechanism; on the contrary, the mechanism in Fig. 5 has a simple structure, but it is more suitable as a passive mechanism. Considering the actuator arrangement, the 8R compliant parallel mechanism is chosen as the final alternative and will be discussed in the following sections.

3 PRBM-based Kinematics

In this section, inverse kinematics of the 8R compliant parallel mechanism is analyzed and the effects of geometrical parameters of the flexure hinge on the kinematic analysis are then discussed. The pseudo-rigid-body model (PRBM) proposed by Howell et al. [2] is used to analyze the kinematics of the 8R compliant parallel mechanism. The PRBM of the 8R compliant mechanism is shown in Fig. 8. Considering the fact that the kinematics of the PRBM is irrelevant to mechanical parameters such as the stiffness of the torsional spring, it has the same as the kinematics of the 8R rigid mechanism in Fig. 1. Thus, the inverse displacement analysis is implemented to verify the rationality of analyzing kinematics of compliant parallel mechanism using the PRBM.

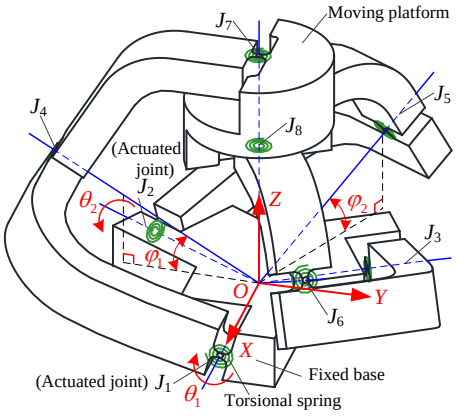

Fig. 8 The PRBM corresponding to the 8R compliant mechanism in Fig. 3

Preliminary researches about the kinematics of the 8R rigid mechanism have been carried out by Kong [18] and Zhang [19]. However, considering the various configurations of 8R mechanism and the convenience of the readers, the inverse kinematic analysis of the 8R mechanism in Fig. 1 is rewritten here.

The unit vector $\boldsymbol{r}_i = (x_i, y_i, z_i)^{\mathrm{T}}$, ($i$=1, 2…8) is used to denote the axial direction of joint J_i. The axis of joint J_4 is orthogonal to that of joint J_1, and the angle θ_0 between the axis of joint J_4 and that of joint J_7 is 60°, thus it can be obtained as

$$\begin{cases} \boldsymbol{r}_4 \cdot \boldsymbol{r}_1 = \cos(\pi/2) \\ \boldsymbol{r}_4 \cdot \boldsymbol{r}_7 = \cos\theta_0 \\ |\boldsymbol{r}_4| = 1 \end{cases} \tag{1}$$

According to Eq. (1), each component of the unit vector $\boldsymbol{r}_4$ can be obtained as

$$x_4 = 0 \tag{2}$$

$$z_4 = \frac{z_7 \cos\theta_0 + y_7\sqrt{\sin^2\theta_0 - x_7^2}}{1 - x_7^2} \tag{3}$$

In the case of $y_7 \neq 0$,

$$y_4 = \frac{1}{y_7}(\cos\theta_0 - z_4 z_7) \tag{4}$$

In the case of $y_7 = 0$,

$$y_4 = -\sqrt{1 - z_4^2} \tag{5}$$

Notice that the axis of joint J_5 is orthogonal to that of joint J_2, and the angle θ_0 between the axis of joint J_5 and that of joint J_7 is 60°, so the unit vector $\boldsymbol{r}_5$ satisfies

$$\begin{cases} \boldsymbol{r}_5 \cdot \boldsymbol{r}_2 = \cos(\pi/2) \\ \boldsymbol{r}_5 \cdot \boldsymbol{r}_7 = \cos\theta_0 \\ |\boldsymbol{r}_5| = 1 \end{cases} \tag{6}$$

According to Eq. (6), each component of the unit vector $\boldsymbol{r}_5$ can be determined as

$$y_5 = \frac{C \pm \sqrt{C^2 - BD}}{B} \tag{7}$$

$$x_5 = -\sqrt{3} y_5 \tag{8}$$

$$z_5 = \frac{1}{z_7}(\cos\theta_0 - x_5 x_7 - y_5 y_7) \tag{9}$$

where $B = A^2 + 4z_7^2$, $C = A\cos\theta_0$, $D = \cos^2\theta_0 - z_7^2$, and $A = y_7 - \sqrt{3}x_7$. Considering the fact that the pitch angle of the moving platform is less than 30°, y_5 in Eq. (7) takes the positive value.

As the unit vector $\boldsymbol{r}_4$ and $\boldsymbol{r}_5$ are known, the angular displacement of actuated joint θ_1, θ_2 can be calculated as

$$\theta_1 = \arccos(-y_4) - \frac{\pi}{6} \tag{10}$$

$$\theta_2 = \arccos\left(-\frac{\sqrt{3}}{2}x_5 + \frac{1}{2}y_5\right) - \frac{\pi}{6} \tag{11}$$

After displacement analysis, the inverse Jacobian Matrix of the 8R compliant mechanism can be further derived to use for its dynamic modelling.

Firstly, the unit vector $\boldsymbol{r}_7$, which denotes the axial direction of the top joint J_7, is written as

$$\boldsymbol{r}_7 = (x_7, y_7, z_7)^{\mathrm{T}} \tag{12}$$

where $x_7 = \sin\gamma\cos\alpha$, $y_7 = \sin\gamma\sin\alpha$, $z_7 = \cos\gamma$.

The unit vector $\boldsymbol{r}_{j+3}$, which denotes the axial direction of the middle joint J_{j+3}, (j=1, 2) is written as

$$\boldsymbol{r}_{j+3} = (x_{j+3}, y_{j+3}, z_{j+3})^{\mathrm{T}} \tag{13}$$

where $x_{j+3} = \cos(\varphi_j + \theta_j)\cos\beta_j$, $y_{j+3} = \cos(\varphi_j + \theta_j)\sin\beta_j$, $z_{j+3} = \sin(\varphi_j + \theta_j)$.

As shown in Fig. 8, θ_j is the angular displacement of the actuated joint J_j, φ_j is the initial value of the angle between the unit vector $\boldsymbol{r}_{j+3}$ and the plane XOY, β_j is the angle between the projection of the unit vector $\boldsymbol{r}_{j+3}$ in the plane XOY and the axis X. In the 8R compliant mechanism, $\varphi_1 = \varphi_2 = \pi/6$, $\beta_1 = -\pi/2$, $\beta_2 = 5\pi/6$.

In the 8R compliant mechanism, the angle between the axis of the middle joint (J_4 and J_5) and that of the top joint (J_7) is always θ_0, it is therefore formulated as

$$\boldsymbol{r}_{j+3} \cdot \boldsymbol{r}_7 = \cos\theta_0 \quad j=1, 2 \tag{14}$$

Taking the derivative of Eq. (14) leads to

$$P_j\dot{\theta}_j = Q_j\dot{\gamma}_j + R_j\dot{\alpha}_j \tag{15}$$

where $P_j = -\sin(\varphi_j + \theta_j)\sin\gamma\cos(\alpha - \beta_j) + \cos(\varphi_j + \theta_j)\cos\gamma$,

$Q_j = -\cos(\varphi_j + \theta_j)\cos\gamma\cos(\alpha - \beta_j) + \sin(\varphi_j + \theta_j)\sin\gamma$,

$R_j = \cos(\varphi_j + \theta_j)\sin\gamma\sin(\alpha - \beta_j)$.

According to Eq. (15), the differential kinematics of the 8R compliant mechanism is obtained as

$$\begin{bmatrix} \dot{\theta}_1 \\ \dot{\theta}_2 \end{bmatrix} = \boldsymbol{J} \begin{bmatrix} \dot{\gamma} \\ \dot{\alpha} \end{bmatrix} \tag{16}$$

where $\boldsymbol{J}$ is the inverse Jacobian Matrix of the 8R compliant mechanism, and

$$\boldsymbol{J} = \begin{bmatrix} \dfrac{Q_1}{P_1} & \dfrac{R_1}{P_1} \\ \dfrac{Q_2}{P_2} & \dfrac{R_2}{P_2} \end{bmatrix} \tag{17}$$

Next, it is necessary to verify whether the inverse kinematic analysis in terms of PRBM is applicable to the compliant mechanism. The processes of verification are listed as follows:

(1) Under the condition that the pitch angle γ and the phase angle α are known, the angular displacements θ_1 and θ_2 of actuated joints J_1 and J_2 are calculated according to the above inverse displacement analysis.

(2) In the finite element model of the 8R compliant mechanism, geometric constraints derived from the angular displacements θ_1, θ_2 are imposed and the new pitch angle γ' and phase angle α' of the moving platform are obtained.

(3) The difference between the angles γ' and γ, or α' and α is compared. In addition, the effect of geometrical parameters of the flexure hinge on the kinematic analysis is analyzed.

Geometrical parameters of the notch flexure hinge are set h=15 mm, t=10 mm, l=5 mm, R=1.75 mm, δ=0.6 mm as a standard flexure hinge. As any parameter of the standard flexure hinge changes, the flexure hinge becomes another case. Considering the ratio of strength and weight of material and the fact that only a limited kinds of material could serve as 3D printing material, take nylon 66 as the material of the flexure hinge. A part of mechanical parameters of nylon 66 are listed as follows: Modulus of elasticity is 3.3 GPa, and Poisson's

ratio is 0.33. In case of γ=10°, α=45°, angular displacements of the two actuated joints are θ_1=7.36° and θ_2=3.09° by solving for Eqs. (10) and (11). The simulation results for flexure hinges with different geometrical parameters are listed in Table 3.

Table 3 Simulation results of flexure hinges with different geometrical parameters

Geometrical parameters	Pitch angle (theoretical value γ=10°)		Phase angle (theoretical value α=45°)	
	Simulation (°)	Relative deviation	Simulation (°)	Absolute deviation (°)
Standard flexure hinge: h=15 mm, t=10 mm, l=5 mm R=1.75 mm, δ=0.6 mm	9.195	8.05%	47.68	2.68
Variable 1：t=15 mm	9.399	6.01%	46.84	1.84
Variable 2：l=8 mm	9.248	7.52%	47.58	2.58
Variable 3：R=2 mm	9.070	9.30%	48.20	3.20
Variable 4：δ=1 mm	8.253	17.47%	51.13	6.13
Variable 5：h=10 mm	8.710	12.90%	48.98	3.98
Devoid of passive limb	9.155	8.45%	47.38	2.38

Seen from Table 3, simulation results from the finite element models are similar to theoretical analysis using the PRBM, which means that it is feasible to analyze kinematics of the 8R compliant mechanism using the PRBM. Moreover, each geometrical parameters of flexure hinge will exert an effect on the simulation results to some extent. It is interesting that the passive limb of the parallel mechanism has no significant effect on the mobility of the platform. However, the passive limb can increase its bearing capacity according to [19, 24].

After analyzing kinematics of the 8R compliant mechanism, the maximum stress of the mechanism existing within the workspace is calculated, it should be less than the allowable stress of the material, which is one significant feature of compliant mechanisms different from rigid mechanisms. Since flexure hinges of the 8R compliant mechanism are designed as the notch flexure hinges, the maximum stress must exist in the flexure hinges. The maximum angular displacements of all joints are firstly obtained when the moving platform rotates within its workspace. Then, the maximum stress of each joint is then figured out on the basis of the maximum angular displacement and geometrical parameters of the flexure hinge.

Assume that the workspace of the mechanism satisfies: $\gamma \in [-10^\circ, +10^\circ]$ and $\alpha \in [0^\circ, 360^\circ)$. When the movement of the moving platform is a uniform circular motion (γ=10°, α=0~360°), the angular displacements of all eight joints with respect to time are illustrated in Fig. 9. Where the period of the uniform circular motion is 1s and "J_i" denotes joint J_i in Fig. 9. The maximum angular displacements of the eight joints are listed in Table 4.

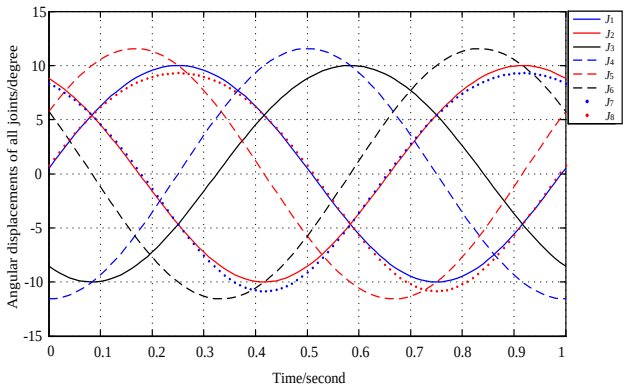

Fig. 9 Angular displacements of all joints vary with time

The data in Table 4 show that the difference between the maximum angular displacements of any two joints is up to at most 15.6%, which signifies that all joints could be replaced with flexure hinges with the same geometrical parameters. For the standard flexure hinge mentioned previously, when its angular displacement reaches 11.56°, the maximum stress of the flexure hinge is 80.9MPa, less than the allowable stress of nylon 66. Therefore, the design of the 8R compliant mechanism whose joints are replaced with the standard flexure hinges is feasible.

In addition, the maximum angular displacements of any two joints in the 8R mechanism are approximate, and the range of pitch angle and the maximum angular displacements of the joints have similar values. Consequently, if the travel range of the flexure hinge increases, the workspace of the 8R compliant mechanism is enlarged proportionally.

Table 4 The maximum angular displacements of all eight joints

Joint	J_1	J_2	J_3	J_4	J_5	J_6	J_7	J_8
The maximum angular displacement/°	10.00	9.998	9.998	11.57	11.56	11.56	10.84	10.84

4 Inverse Dynamic Simulation Considering Joint Damping

In this section, inverse dynamics of the 8R compliant mechanism is analyzed, which is used to select actuators of the mechanism. As a general rule, Structural dynamics is used to model the compliant mechanism and analyze its inverse dynamics. Many researchers [25-29] have been engaged in the dynamic analysis and modelling of the parallel kinematic machines or flexible manipulators. Given the complexity of the 8R compliant parallel mechanism, however, its inverse dynamics is analyzed with aid of the virtual prototyping software ADAMS, which makes it easy to select actuators of the mechanism reasonably. Specifically, both inverse dynamic simulation and actuator selection are implemented in the framework of PRBM.

In Fig. 8, the stiffness of the torsional spring equals to the rotational stiffness of the flexure hinge. However, for a general PRBM, whether its dynamic analysis needs to consider joint damping caused by the material damping is a question worthy to be discussed. Generally, joint damping is not taken into consideration in the existing PRBM because it is traditionally believed to be negligible. Without joint damping, however, the vibration of the moving platform is inevitable when the driving torque is imposed on the actuated joints. Consequently, the PRBM without considering the existence of joint damping is inconsistent with its physical prototype.

In this section, joint damping of the flexure hinge is taken into account in the inverse dynamic simulation of the 8R compliant mechanism. Firstly, a method to determine joint damping of the flexure hinge is presented. Then under the condition of the known joint damping, the effect of joint damping on actuator selection and real-time control is further discussed as joint damping known.

4.1 Determination of Joint Damping

In general, there are two methods to determine joint damping of the flexure hinge. One is prototype experiment and the other is the finite element simulation under the condition of known material damping. The result of the first method is authentic and precise in terms of the experimental data; while the result of the second method on the basis of the finite element simulation is obtained easily and usually used as a reference. Considering the ease of implementation and the gradual advance of research, the second method is used to acquire joint damping of the flexure hinge. The process of obtaining joint damping is listed as follows:

(1) Static analysis of the finite element model is used to obtain the rotational stiffness of the flexure hinge.

(2) Dynamic analysis of the finite element model is used to obtain step response of the flexure hinge.

(3) According to theoretical analysis of step response of a second-order system, the step response curves with respect to different damping ratio are drawn.

(4) The step response curve closest to the simulation result could be used to acquire joint damping of the flexure hinge.

Assume that the flexure hinge is made of nylon 66. The remaining mechanical parameters of nylon 66 except those mentioned in Section 3 are listed as follows: the density is 1150 kg/m^3, the material damping is 0.05. New geometrical parameters of the flexure hinge are assigned as: L=15mm, h=15 mm, t=10 mm, l=5 mm, R=1.75 mm, δ=0.6 mm. Firstly, the finite element software ANSYS is used to obtain the rotational stiffness K of the flexure hinge, which is also the stiffness of the torsional spring in the PRBM. Thus, the rotational stiffness K

is 4.78N·mm/°. Secondly, the step response curve of the flexure hinge is acquired by dynamic analysis function in ANSYS, which is illustrated in Fig. 10. Note that joint damping of the flexure hinge can be further obtained by fitting the simulation result. By fitting the step response curve, as shown in Fig. 10, joint damping D of the flexure hinge is finally determined and its value is 0.226 N·mm·s/°.

Next, keep geometrical parameters of the notch in the flexure hinge constant and other parameters be changed, where L=20 mm, h=20 mm. Rotational stiffness and joint damping of the new flexure hinge are obtained in a similar way, where the rotational stiffness K=4.80 N·mm/°, and the joint damping D=0.229 N·mm·s/°. By comparing the values obtained in the two groups of simulations, it is concluded that rotational stiffness and joint damping of the flexure hinge mainly depend on geometrical parameters of the flexural notch. As a result, the notch flexure hinge could be equivalently replaced by the joint with a damping torsional spring.

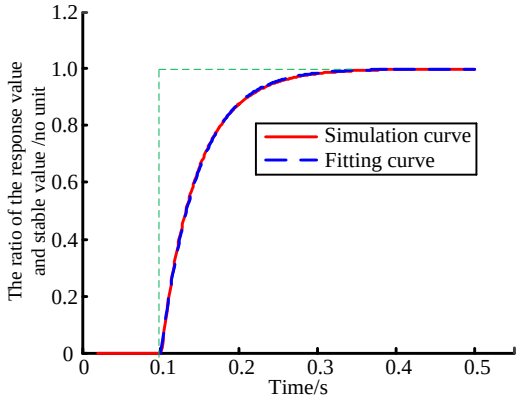

Fig. 10 Simulation curve and fitting curve using the software ANSYS for a step response

4.2 Dynamic Simulation Considering Joint Damping

Now select the stiffness K of the torsional spring is 4.78N·mm/°, and the joint damping D is 0.226N·mm·s/° for the flexure hinges in the PRBM in Fig. 8, the dynamic simulation of the PRBM is then carried out using the virtual prototype software ADAMS, which is used for actuator selection and real-time control.

First of all, the PRBM in Fig. 8 is imported into ADAMS. Assume that the motion of the moving platform is uniform circular motion in which the period is one second. In the circular motion, the pitch angle γ is 10°, the range of phase angle α is 0~360°. After the simulation is completed, two input torques imposed on the two actuated joints are measured, which are shown in Fig. 11, where, "T_{J1}", "T_{J2}" denote input torques of the actuated joints J_1, J_2 respectively; the suffixes "-dl", "-no" signify the simulation with and without considering joint damping, respectively. The difference between input torques corresponding to the two

cases is shown in Fig. 12 where "DT_{Ji}" denotes input torque difference of the actuated joint J_i, (i=1 or 2).

By analyzing the curves in Fig. 11, it is observed that the maximum input torques of the actuated joints are close to each other both in the case of considering or not considering joint damping, as shown in Table 5. As a result, joint damping has little effect on the actuator selection. But from the point view of real-time control, joint damping is not negligible because input torque difference corresponding to the two cases are up to at most 86.40 N·mm, which accounts for 28.45% (86.4/303.7) of the maximum input torque of the actuated joints.

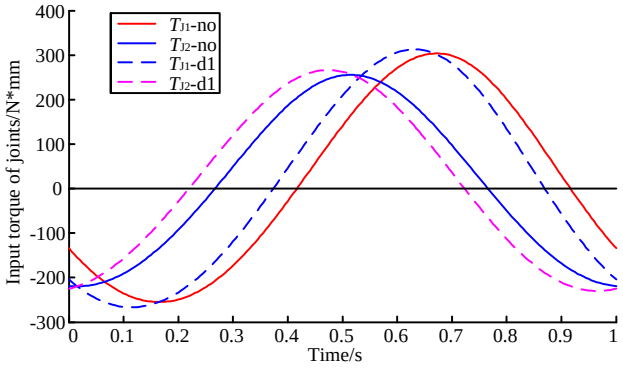

Fig. 11 Input torques curve of the actuated joints varying with respect to time

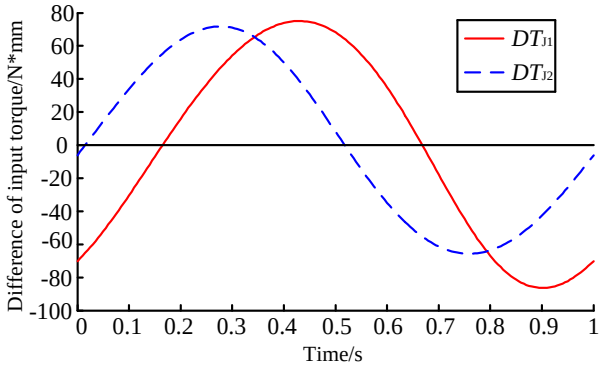

Fig. 12 Input torque differences of the two cases varying with time

Table 5 The maximum input torques of the actuated joints

Actuated joint	No damping	Considering damping	Relative deviation
J_1	303.7 N·mm	312.9 N·mm	3.03%
J_2	255.6 N·mm	266.4 N·mm	4.21%

5 Summary

In this paper, a notch-type 8R compliant parallel mechanism with two rotational DOFs is designed to meet the requirement of a lightweight and compact pan-tilt platform. Firstly, the two commonly-used design approaches i.e. direct substitution and FACT are used to

determine topology and configuration of the pan-tilt systems, and the similarities and differences between two design candidates are compared. The mechanism obtained by using the direct substitution method is more suitable to use as the active mechanism; on the contrary, the resultant mechanism obtained from FACT approach is more suitable to use as the passive mechanism. After completing the conceptual design of an 8R compliant parallel pan-tilt platform, its kinematics is analyzed by using the PRBM approach and the mechanism's maximum stress within the workspace is tested by finite element analysis software ANSYS. The analysis result shows that kinematic analysis deviation of the compliant parallel mechanism using the PRBM can be limited within an acceptable value. Furthermore, the maximum angular displacements of all joints and the maximum pitch angle of the moving platform are similar in value, which might guide the design and stress analysis of the 8R mechanism. Finally, the issue on joint damping in the flexure hinge is explored. To the authors' best knowledge, almost no existing literature talks about this issue. With the aid of finite element software ANSYS and virtual prototype software ADAMS, it is concluded that joint damping is negligible for actuator selection but not negligible for real-time control in the case study.

Acknowledgements

The authors gratefully acknowledge the financial support of the National Natural Science Foundation of China under Grant No. 51175010 and Ph.D. Programs Foundation of Education of China under Grant No. 20111102130004.

References

1. Her, I., and Midha, A., 1987, "A compliance number concept for compliant mechanisms, and type synthesis," *ASME Journal of Mechanisms, Transmissions, and Automation in Design*, 109(3), pp. 348-355.
2. Howell, L.L., 2001, *Compliant mechanisms*, John Wiley & Sons, Hoboken, NJ.
3. Tlusty, J., Ziegert, J., and Ridgeway, S., 1999. "Fundamental comparison of the use of serial and parallel kinematics for machines tools," *CIRP Annals-Manufacturing Technology*, 48(1), pp. 351-356.
4. Wenger, P., Gosselin, C., and Maille, B., 1999, "A comparative study of serial and parallel mechanism topologies for machine tools," *Proc. PKM'99*, pp. 23-32.
5. Hara, A., and Sugimoto, K., 1989, "Synthesis of parallel micromanipulators," *ASME Journal of Mechanisms, Transmissions and Automation in Design*, 111(1), pp. 34-39.
6. Yu, J. J., Bi, S. S., and Zong, G. H., 2004, "A method to evaluate and calculate the mobility of a general compliant parallel manipulator," *ASME 2004 International Design Engineering*

Technical Conferences and Computers and Information in Engineering Conference, pp. 743-748.

7. Bruzzone, L., and Molfino, R. M., 2006, "A novel parallel robot for current microassembly applications, " *Assembly Automation*, 26(4), pp. 299-306.
8. Dong, W., Sun, L. N., and Du, Z. J., 2007, "Design of a precision compliant parallel positioner driven by dual piezoelectric actuators," *Sensors and Actuators A: Physical*, 135(1), pp. 250-256.
9. Hao, G. B., Kong, X. W., and Meng, Q., 2010, "Design and modelling of spatial compliant parallel mechanisms for large range of translation," *ASME 2010 International Design Engineering Technical Conferences and Computers and Information in Engineering Conference*, pp. 329-340.
10. Palpacelli, M. C., Palmieri, G., and Callegari, M, 2012, "A Redundantly actuated 2-degrees-of-freedom mini pointing device. *ASME Journal of Mechanisms and Robotics*," 4(3), pp. 031012.
11. Hopkins, J. B., and Culpepper, M. L., 2010, "Synthesis of multi-degree of freedom, parallel flexure system concepts via Freedom and Constraint Topology (FACT)–Part I: Principles," *Precision Engineering*, 34(2), pp. 259-270.
12. Yu, J.J., Li, S. Z., Su, H. J., and Culpepper, M. L., 2011, "Screw theory based methodology for the deterministic type synthesis of flexure mechanisms," *ASME Journal of mechanisms and robotics*, 3(3), pp. 031008.
13. Ball, R.S. 1900, *A Treatise on the Theory of Screws*, Cambridge University Press, Cambridge.
14. Lobontiu, N. 2003, *Compliant Mechanisms: Design of Flexure Hinges*. Boca Raton: CRC Press
15. Trease, B.P., Moon Y, Kota S. 2005, "Design of large-displacement compliant joints," *ASME Journal of Mechanical Design*. 127(7): 788-798.
16. Ouerfelli, M., and Kumar, V., 1994, "Optimization of a spherical five-bar parallel drive linkage," *ASME Journal of Mechanical Design*, 116(1), pp. 166-173.
17. Zhang, L. J., Niu, Y. W., Li, Y. Q., and Huang, Z., 2006, "Analysis of the workspace of 2-DOF spherical 5R parallel manipulator," *Robotics and Automation, 2006. Proceedings of the 2006 IEEE International Conference on Robotics and Automation*, pp. 1123-1128.
18. Kong, X. W., 2010, "Forward displacement analysis of a 2-DOF RR-RRR-RRR spherical parallel manipulator," *Mechatronics and Embedded Systems and Applications (MESA), 2010 IEEE/ASME International Conference*, pp. 446-451.
19. Zhang, L. J., Niu, Y. W., and Huang, Z., 2006, "Analysis of the workspace of spherical 2-dof parallel manipulator with actuation redundancy," *Mechatronics and Automation, Proceedings of the 2006 IEEE International Conference*, pp. 153-158.
20. Sofka, J., Skormin, V., Nikulin, V., and Nicholson, D. J., 2006, "Omni-Wrist III-a new

generation of pointing devices. Part I. Laser beam steering devices-mathematical modeling," *IEEE Transactions on Aerospace and Electronic Systems*, 42(2), pp. 718-725.

21. Yu, J. J., Dong, X., Kong, X. W., and Pei, X., 2012, "Mobility and singularity analysis of a class of two degrees of freedom rotational parallel mechanisms using a visual graphic approach," *ASME Journal of Mechanisms and Robotics*, 4(4), pp. 041006.
22. Lobontiu, N., Garcia, E., Goldfarb, M., and Paine, J. S., 2001, "Corner-filleted flexure hinges," *ASME Journal of Mechanical Design*, 123(3), pp. 346-352.
23. Smith, S. T., Badami, V. G., Dale, J. S., and Xu, Y., 1997, "Elliptical flexure hinges," *Review of Scientific Instruments*, 68(3), pp. 1474-1483.
24. Wu, J., Li, T. M., Wang, J. S., and Wang, L. P., 2013, "Stiffness and natural frequency of a 3-DOF parallel manipulator with consideration of additional leg candidates," *Robotics and Autonomous Systems*, 61(8), pp. 868-875.
25. Cammarata, A., Condorelli, D., and Sinatra, R., 2013, "An algorithm to study the elastodynamics of parallel kinematic machines with lower kinematic pairs," *ASME Journal of Mechanisms and Robotics*, 5(1), 011004.
26. Bratland, M., Haugen, B., and Rølvåg, T., 2011, "Modal analysis of active flexible multibody systems," *Computers & Structures*, 89(9), pp. 750-761.
27. Jonker, B., 1990, "A finite element dynamic analysis of flexible manipulators," The *International Journal of Robotics Research*, 9(4), pp. 59-74.
28. Palmieri, G., Martarelli, M., Palpacelli, M. C., and Carbonari, L., 2014, "Configuration-dependent modal analysis of a Cartesian parallel kinematics manipulator: numerical modeling and experimental validation," *Meccanica*, 49(4), pp. 961-972.
29. Bricout, J. N., Debus, J. C., and Micheau, P., 1990, "A finite element model for the dynamics of flexible manipulators," *Mechanism and Machine Theory*, 25(1), pp. 119-128.